ChemComm

Accepted Manuscript

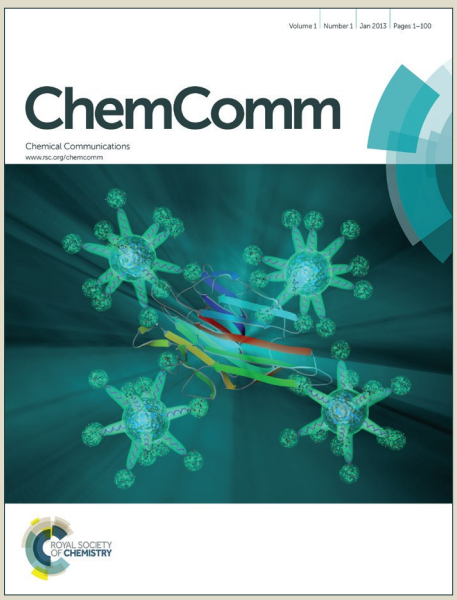

ROYAL SOCIETY OF CHEMISTRY

www.rsc.org/chemcomm

Cite this: DOI: 10.1039/c0xx00000x

www.rsc.org/xxxxxx

ARTICLE TYPE

Self-assembled arrays of polyoxometalate-based metal–organic nanotubes for proton conduction and magnetism

Yan-Qing Jiao, Hong-Ying Zang, Xin-Long Wang*, En-Long Zhou, Bai-Qiao Song, Chun-Gang Wang*, Kui-Zhan Shao, Zhong-Min Su*

Received (in XXX, XXX) Xth XXXXXXXXX 20XX, Accepted Xth XXXXXXXXX 20XX
DOI: 10.1039/b000000x

The first polyoxometalate-based metal–organic nanotube constructed *via* covalent bonds has been synthesized. POMs anions stick the metal–organic nanotubes to build 3D nanotubular arrays. The stability, magnetic and proton conducting properties are investigated.

Since the pioneering discovery of carbon nanotubes (CNTs) by Iijima in 1991,[1] design and synthesis of discrete nanotubular materials have attracted tremendous scientific interest not only due to their intriguing architectures and characteristic electronic structures, but also owing to their potential applications in gas storage, drug delivery, catalyst and molecular recognition.[2] However, the harsh synthetic conditions definitely hinder the development of such fascinating materials.[2a] In contrast, metal–organic frameworks (MOFs), as a significant class of porous materials, with diverse topological architecture and specific pore surfaces have become a research hotspot and developed dramatically.[3] However, only few metal–organic nanotubes (MONTs) have been reported to date, especially discrete MONTs.[4] Given that MOFs exhibit a few weak points such as poor chemical stability,[3h] the design and synthesis of such MONTs with high chemical stability is one of the most challenging issues in synthetic chemistry.

Polyoxometalates (POMs) as well known as a diverse class of discrete anionic metal oxides can serve as transferable building blocks that can be applied in the preparation of functional materials, due to their nanosize and tunable acid/base, redox, magnetic, catalytic, and photochemical properties.[5] Recently, a great deal of attention has been focused on the fabrication of polyoxometalate-based metal–organic frameworks (POMOFs), which merge the merits of POMs and MOFs, thus endowing them with new features and multiple functionalities distinctively different from the POMs or MOFs alone.[6] Inspired by this, we envisaged that the introduction of POMs to MONTs might achieve new types of porous materials possessing both versatility and stability. Additionally, attempts to prepare porous POMOFs have met with only limited success especially for POM-based metal-organic nanotubes.[7] Indeed, we are aware of only one example, that is, POM-organic supermolecular nanotubes has been reported to date.[8]

Herein, we succeeded in constructing an assembly of unique POM-based MONTs $[Cu_3(\mu_3\text{-}OH)(H_2O)_3(atz)_3]_3[P_2W_{18}O_{62}]\cdot 14H_2O$ (**1**, Hatz = 3-amino-1,2,4-triazolate) that was synthesized by hydrothermal reaction of $CuCl_2$, Hatz and $\alpha\text{-}K_6P_2W_{18}O_{62}\cdot 15H_2O$ at 140 °C for 3 days. The formula of **1** was figured out on the basis of microanalysis and thermogravimetric analysis (TGA) results (Fig. S1). The phase purity of bulk product was testified by a comparison of the experimental X-ray powder diffraction (XRPD) pattern with the simulated pattern from single-crystal X-ray diffraction (Fig. S2). As expected, **1** exhibits exceptional chemical and thermal stability. Unlike most POMOFs with POMs as nodes, POMs in **1** just act as linkers, holding these MONTs together to form 3D nanotubular arrays. To the best of our knowledge, 3D POM-based MONTs assembled by covalent bonds have not been reported so far.

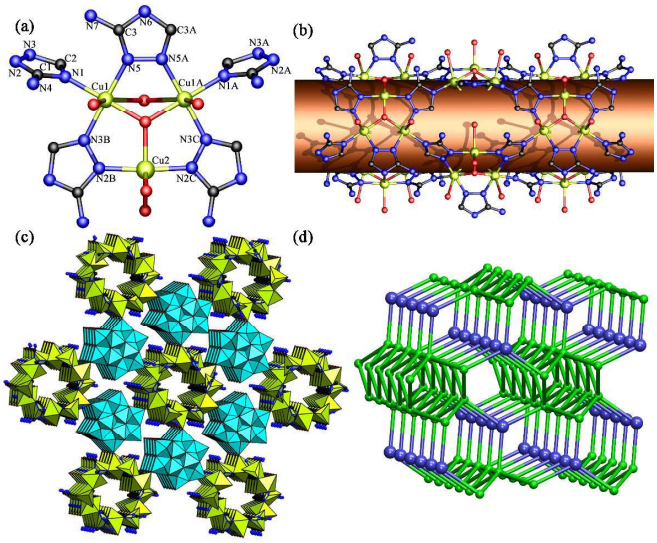

Fig. 1 Crystal structures of **1**: (a) Stick view of triangular Cu3-triad units; (b) Perspective view of the 1D single-walled nanotube in **1**; (c) The 3D nanotubular framework of **1** viewed along c-axis; (d) The topological of 3D network. Symmetry operation: A: -y, - *x*+*y*, -*z*; B: *x*, *y*, -0.5-*z*; C: *x*, *y*, *z*.

Single crystal X-ray diffraction analysis (Table S1) reveals that **1** crystallizes in the hexagonal system with space group $P6_3/m$ and possesses a nanotubular framework. As shown in Fig. 1, the structure contains two kinds of motifs: $\{P_2W_{18}\}$ polyanions and $[Cu_3(\mu_3\text{-}OH)(H_2O)_3(atz)_3]^{2+}$ cations. Analysis of the local symmetry of the atoms shows that the Cu2 center resides on a

special position (site occupancy factor (SOF) = 0.5) containing a twofold axis of rotation, and the P center lies on the other special symmetry site (SOF = 1/3) containing a three-fold axis of rotation. One of the atz ligand is also located on a two-fold axis, causing a two-fold disorder of this ligand throughout the crystal structure. There are two kinds of crystallographical independent copper atoms. The Cu1 center is in the octahedral coordination sphere, bonded to three N atoms from two atz ligands (average Cu–N distance of 1.99(3) Å), one μ_3-O atom (Cu–O 2.02(0) Å) and one terminal O atom derived from P_2W_{18} anion (Cu–O 2.51(8) Å), as well as one water molecule (Cu–O_W 2.81(2) Å). The Cu2 atom displays a five-coordinate square pyramidal coordinated geometry with two N atoms of two atz ligands (Cu–N 1.95(3) Å), one μ_3-O atom (Cu–O 2.02(9) Å) and two coordinated water molecules (average Cu–O_W distance of 2.18(2) Å). Three copper atoms are linked by three atz ligands through N1, N2-bridging mode to form a trinuclear triangular cluster $[Cu_3(\mu_3\text{-}OH)(H_2O)_3(atz)_3]^{2+}$ (Fig. 1a) with a μ_3-O atom occupying a special position with site symmetry twofold axis. The bond valence sum (BVS) calculations[9] show that it belongs to OH group. Each trinuclear cluster $[Cu_3(\mu_3\text{-}OH)(H_2O)_3(atz)_3]^{2+}$, which functions as second building unit, is connected with four neighboring others by sharing four atz ligands, giving rise to a single-walled metal–organic nanotube (Fig. 1b) with an exterior wall diameter of 15.73(2) Å and an interior channel diameter of 8.54(5) Å. Water molecules are located within the interiors of the nanotubes at two crystallographically unique positions (O1W and O2W), which are connected together by multiple strong hydrogen bonds (O1W···O2W 3.24(4) Å; O2W···O2W 2.97(8) Å) to generate 1D hydrogen-bonding water chain (Fig. S3 and Table S2). Meanwhile, each $[Cu_3(\mu_3\text{-}OH)(H_2O)_3(atz)_3]^{2+}$ fragment is covalently bonded to one $\{P_2W_{18}\}$ anion, while each $\{P_2W_{18}\}$ anion provides six terminal O atoms in the equatorial plane to coordinate with three $[Cu_3(\mu_3\text{-}OH)(H_2O)_3(atz)_3]^{2+}$ motifs derived from three neighboring metal–organic nanotubes, thereby constructing an unprecedented 3D architecture (Fig. 1c), which represents the first example of polyoxometalate-based metal-organic nanotubes. To comprehend the structure better, the 3D structure can be rationalized as a (3, 5)-connected network with point symbol $\{4^4\cdot6^6\}_3\{6^3\}$, if we assign the P_2W_{18} cluster as a 3-connected node and the $[Cu_3(\mu_3\text{-}OH)(H_2O)_3(atz)_3]^{2+}$ subunit as 5-connected node (Fig. 1d).

In **1**, the oxidation states of all P, W and Cu atoms are +5, +6, and +2, respectively, based on the charge balance consideration and bond valence sum calculations (the BVS calculation results of all the oxygen atoms and metal atoms in **1** are listed in the Supplementary Information Tables S3–5). The XPS spectrum (Fig. S4) gives two peaks at 953.1 and 933.3 eV, which can be ascribed to Cu^{2+} $2p_{1/2}$ and $2p_{3/2}$, respectively.[10]

As previously mentioned, the stability of MONTs limits the practical application. The thermal stability of **1** has been measured by thermogravimetric analysis (TGA). The TGA curve (Fig. S1) reveals that *ca.* 3.6 % weight loss occurred immediately upon heating and was completed before the temperature reached 130 °C, and this weight loss is indicative of the loss of all lattice water molecules (calcd 3.9 %). On further heating, the materials lose weight continuously during the second step with a weight loss of 3.1 % (calcd 3.5 %), due to the removal of the coordinated water molecules. Above 300 °C, the whole framework collapses with the release of nine Hatz ligands (calcd 12.3 %). Besides, compound **1** also exhibits amazing chemical stability. After being refluxed in boiling water and organic solvents (CH_3OH, C_2H_5OH, acetone, acetonitrile, DMF and DMA) for 3 days, **1** remains its structural integrity, as shown in Fig. S2. Strikingly, after immersed in a hydrochloric acid solution (pH = 2) or sodium hydroxide solution (pH = 12) for 20 h, the XRPD patterns exhibit similar shape and intensity (Fig. S5). As shown in Fig. S6, PXRD patterns for samples heated in flowing N_2 from 100 to 350 °C further confirmed that the structural integrity of the framework remains unchanged until 250 °C. Thus, **1** shows an exceptional resistance to acid/base aqueous solutions, and such high acid/base stability is also very rare in reported MONTs.

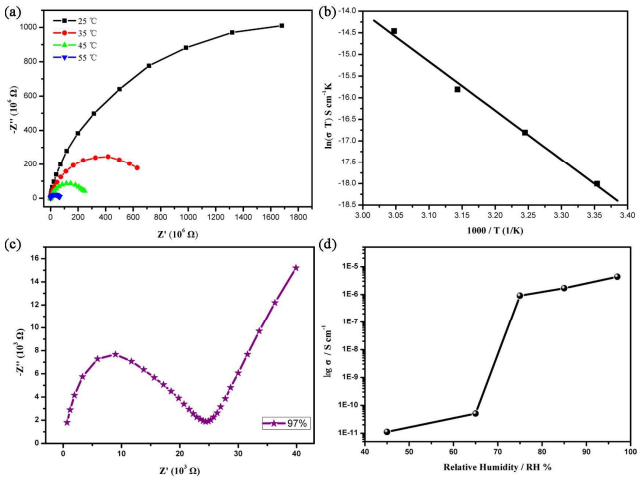

Fig. 2 (a) Nyquist plot for **1** at various temperatures under 65% RH; (b) Arrhenius-type plot of the conductivity of **1** at various temperatures under 65% RH; (c) Impedance spectra (25 °C, 97% RH) of **1**; (d) RH dependence of the conductivity (σ) for **1** at 298 K.

In the crystal structure of **1**, there are water molecules encapsulated in the nanotubes, which makes **1** a promising candidate to be used as a proton conductor with potential applications in fuel cell technology. Besides, the vapour adsorption experiment (Fig. S7 and Fig. S8) suggests that certain amounts of water are adsorbed. Thus, the proton conduction behavior of **1** was studied by alternating current (AC) impedance measurements using a compacted pellet of the powdered crystalline sample. The conductivity of compound **1** at 25 °C is 5.1×10^{-11} S cm^{-1} (65% RH). As temperature rises (Fig. 2a and Fig. S9), the conductivity increases to 1.6×10^{-9} S cm^{-1} under 65% RH at 55 °C. The enhanced conductivities are ascribed to the elevated temperatures, which may not only accelerate proton transition within channels, but promote the dissociation of protons from Hatz cations for water molecules to form H_3O^+ ions. The activation energy at 65% RH is estimated to be 0.33 eV (Fig. 2b), indicating proton conductivity follows chiefly the Grotthuss proton hopping mechanism.[11] The humidity dependence of proton conductivities is shown in Fig. S10. The conductivities are evaluated by semicircle fittings of the Nyquist plots. These values are highly humidity-dependent and increased from 1.1×10^{-11} S cm^{-1} under 45% RH to 4.4×10^{-6} S cm^{-1} under 97% RH at 25 °C (Fig. 2c), respectively. As shown in Fig. 2d, as the relative humidity increases from 65% to near 75%, the proton

conductivity shows an exponential increasing trend. Hence, RH appears to be a significant factor in determining the conductivity of **1**. Very recently, Zheng *el at.* have reported a novel POM-organic supermolecular nanotube with the proton conductivity of 4.0×10^{-7} S cm^{-1} at 25 °C under 98% RH,[8] which is lower than that of **1** (4.4×10^{-6} S cm^{-1} at 25 °C under 97% RH). The differences come from the effective proton-conduction pathways. The nanotubes in **1** are occupied by 1D hydrogen-bonding water chain. Besides, multiple hydrogen bonds (Table S2) among POM oxygen atoms and atz ligands as well as water molecules construct 3D H-bonding network (Fig. S11), which is conducive to proton conduction. As reported, POMs can strengthen the scaffold, fill void space, provide mobile protons, and improve the hydrophilicity and water retention of the hybrid material.

As illustrated in the literature, the highest occupied molecular orbital (HOMO) and the lowest unoccupied molecular orbital (LUMO) are composed of oxygen 2p and metal d orbitals, respectively.[12] The diffuse reflectance UV–vis spectrum (Fig. S12) of the powder sample **1** was recorded with the corresponding well-defined optical adsorption associated with HOMO–LUMO gap (E),[13] which can be assessed at 2.31 eV (Fig. S13), revealing the band gap of **1** falls into the range of semiconductor.

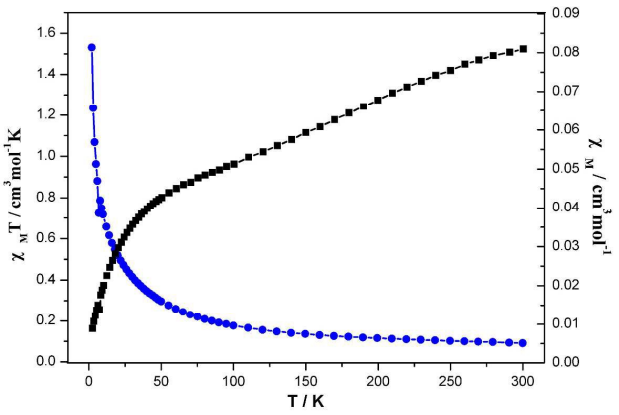

Fig. 3 Plot of temperature dependence of χ_MT (black square) and χ_M (blue dot) versus T for **1** measured under an applied dc magnetic field of 1 kOe.

The temperature-dependent magnetic susceptibility of **1** was measured at 2–300 K with an applied field of 1 KOe for the fresh sample. As shown in Fig. 3, at 300 K, the $\chi_M T$ product is 1.55 cm^3·K·mol^{-1}, smaller than the value of 3.38 cm^3·K·mol^{-1} expected for nine uncoupled Cu^{2+} ions with a reasonable g-value ($S = 1/2$).[14] With temperature dropping, the $\chi_M T$ value decreases continuously down to a value of 0.81 cm^3·K·mol^{-1} at 50 K. As the temperature decreases, the $\chi_M T$ value starts to decreases rapidly, reaching 0.16 cm^3·K·mol^{-1} at 2 K. This behavior indicates the significant antiferromagnetic exchange interactions. The temperature dependence of the reciprocal susceptibilities χ_M^{-1} (Fig. S14) follows the Curie-Weiss law above 130 K with negative $\theta = -182.78$ K, which supports the presence of dominant antiferromagnetic coupling interactions between spin carriers, as is mentioned above. The Curie constants C = 2.46 cm^3·K·mol^{-1} are reasonable for nine Cu^{2+} ions per formula.

In conclusion, we have designed and synthesized a novel polyoxometalate-based MOF $[Cu_3(\mu_3\text{-}OH)(H_2O)_3(atz)_3]_3[P_2W_{18}O_{62}]\cdot 14H_2O$ (**1**), consisting of an infinite single-walled metal–organic nanotube. These MONTs are covalently held together by the Dawson-type cluster $\{P_2W_{18}\}$, leading to unique nanotubular arrays. Notably, **1** represents the first example of polyoxometalate-based MONTs based on the formation of covalent bonds, in which POMs serve as linkers connecting the neighboring MONTs. Compared with traditional MONTs, **1** has better stability, proton conductivity which can be potentially used in fuel cells.

Acknowledgements

This work was financially supported by the NSFC of China (No. 21471027, 21171033, 21131001, 21222105, 21471028), National Key Basic Research Program of China (No. 2013CB834802), Changbai mountain scholars of Jilin Province and FangWu distinguished young scholar of NENU. The Fundamental Research Funds for the Central Universities (No. 2412015KJ012). We thank the reviewers for their helpful comments.

Notes and references

Institute of Functional Material Chemistry, Key Lab of Polyoxometalate Science of Ministry of Education, Faculty of Chemistry, Northeast Normal University, Changchun 130024, P. R. China. Fax: +86-431-85684009; Tel: +86-431-85099108. E-mail:wangxl824@nenu.edu.cn; wangcg925@nenu.edu.cn; zmsu@nenu.edu.cn.

† Electronic Supplementary Information (ESI) available: XRPD, TGA, UV-vis absorption spectrum, Tables, X-ray crystallographic files in CIF format. See DOI:10.1039/b000000x/

1. S. Iijima, *Nature*, 1991, **354**, 56.
2. (a) K. Otsubo, Y. Wakabayashi, J. Ohara, S. Yamamoto, H. Matsuzaki, H. Okamoto, K. Nitta, T. Uruga and H. Kitagawa, *Nat. Mater.*, 2011, **10**, 291; (b) M. Fujita, M. Tominaga, A. Hori and B. Therrien, *Acc. Chem. Res.*, 2005, **38**, 369; (c) J. R. Li, Q. Yu, Y. Tao, X. H. Bu, J. Ribas and S. R. Batten, *Chem. Commun.*, 2007, 2290; (d) C. Y. Sun, C. Qin, C. G. Wang, Z. M. Su, S. Wang, X. L. Wang, G. S. Yang, K. Z. Shao, Y. Q. Lan and E. B. Wang, *Adv. Mater.*, 2011, **23**, 5629; (e) G. Q. Kong, S. Ou, C. Zou and C. D. Wu, *J. Am. Chem. Soc.*, 2012, **134**, 19851.
3. (a) B. F. Abrahams, B. F. Hoskins, D. M. Michail and R. Robson, *Nature*, 1994, **369**, 727; (b) O. M. Yaghi, G. Li and H. Li, *Nature*, 1995, **378**, 703; (c) H. Li, M. Eddaoudi, M. O'Keeffe and O. M. Yaghi, *Nature*, 1999, **402**, 276; (d) Q. L. Zhu and Q. Xu, *Chem Soc Rev*, 2014, **43**, 5468; (e) J. Liang, X. L. Wang, Y. Q. Jiao, C. Qin, K. Z. Shao, Z. M. Su and Q. Y. Wu, *Chem. Commun.*, 2013, **49**, 8555; (f) M. Zhao, S. Ou and C. D. Wu, *Acc. Chem. Res.*, 2014, **47**, 1199; (g) M. Eddaoudi, D. F. Sava, J. F. Eubank, K. Adil and V. Guillerm, *Chem. Soc. Rev.*, 2015, **44**, 228; (h) W. Zhang, Y. Hu, J. Ge, H. L. Jiang and S. H. Yu, *J. Am. Chem. Soc.*, 2014, **136**, 16978.
4. (a) F. Dai, H. He and D. Sun, *J. Am. Chem. Soc.*, 2008, **130**, 14064; (b) T. T. Luo, H. C. Wu, Y. C. Jao, S. M. Huang, T. W. Tseng, Y. S. Wen, G. H. Lee, S. M. Peng and K. L. Lu, *Angew. Chem. Int. Ed.*, 2009, **48**, 9461; (c) G. Wu, J. Bai, Y. Jiang, G. Li, J. Huang, Y. Li, C. E. Anson, A. K. Powell and S. Qiu, *J Am Chem Soc*, 2013, **135**, 18276; (d) D. K. Unruh, K. Gojdas, A. Libo and T. Z. Forbes, *J. Am. Chem. Soc.*, 2013, **135**, 7398; (e) T. W. Tseng, T. T. Luo and K. H. Lu, *CrystEngComm*, 2014, **16**, 5516.
5. (a) M. T. Pope, *Heteropoly and Isopoly Oxometalates*, Springer-Verlag: New-York, 1983; (b) E. Coronado and C. J. Gómez-García, *Chem. Rev.*, 1998, **98**, 273; (c) A. Dolbecq, E. Dumas, C. R. Mayer and P. Mialane, *Chem. Rev.*, 2010, **110**, 6009; (d) H. N. Miras, L. Vila-Nadal and L. Cronin, *Chem. Soc. Rev.*, 2014, **43**, 5679; (e) Y. Q. Jiao, C. Qin, H. Y. Zang, W. C. Chen, C. G. wang, T. T. Zheng, K. Z. Shao and Z. M. Su, *CrystEngComm*, 2015, 17, 2176; (f) Y. Q. Jiao, C. Qin, C. Y. Sun, K. Z. Shao, P. J. Liu, P. Huang, K. Zhou and Z. M. Su, *Inorg. Chem. Commun.*, 2012, **20**, 273; (g) S. T. Zheng and G. Y. Yang, *Chem. Soc. Rev.*, 2012, **41**, 7623.

6. (a) D. Y. Du, J. S. Qin, S. L. Li, Z. M. Su and Y. Q. Lan, *Chem. Soc. Rev.*, 2014, **43**, 4615; (b) Q. Han, X. Sun, J. Li, P. Ma and J. Niu, *Inorg. Chem.*, 2014, **53**, 6107; (c) B. Nohra, H. El Moll, L. M. Rodriguez Albelo, P. Mialane, J. Marrot, C. Mellot-Draznieks, M. O'Keeffe, R. Ngo Biboum, J. Lemaire, B. Keita, L. Nadjo and A. Dolbecq, *J. Am. Chem. Soc.*, 2011, **133**, 13363.
7. (a) H. Fu, C. Qin, Y. Lu, Z. M. Zhang, Y. G. Li, Z. M. Su, W. L. Li and E. B. Wang, *Angew. Chem. Int. Ed.*, 2012, **51**, 7985; (b) F. J. Ma, S. X. Liu, C. Y. Sun, D. D. Liang, G. J. Ren, F. Wei, Y. G. Chen and Z. M. Su, *J. Am. Chem. Soc.*, 2011, **133**, 4178; (c) J. Song, Z. Luo, D. K. Britt, H. Furukawa, O. M. Yaghi, K. I. Hardcastle and C. L. Hill, *J. Am. Chem. Soc.*, 2011, **133**, 16839; (d) D. Shi, C. He, B. Qi, C. Chen, J. Niu and C. Duan, *Chem. Sci.*, 2015, **6**, 1035.
8. G. J. Cao, J. D. Liu, T. T. Zhuang, X. H. Cai and S. T. Zheng, *Chem. Commun.*, 2015, 51. 2048.
9. I. D. Brown and D. Altermatt, *Acta Crystallogr., Sect. B*, 1985, **41**, 244.
10. (a) H. Y. Liu, H. Wu, J. Yang, Y. Y. Liu, B. Liu, Y. Y. Liu and J. F. Ma, *Cryst. Growth Des.*, 2011, **11**, 2920; (b) J. Chen, J. Q. Sha, J. Peng, Z. Y. Shi, B. X. Dong and A. X. Tian, *J. Mol. Struct.*, 2007, **846**, 128; (c) G. G. Jang, C. B. Jacobs, R. G. Gresback, I. N. Ivanov, I. I. I. H. M. Meyer, M. Kidder, P. C. Joshi, G. E. Jellison, T. J. Phelps, D. E. Graham and J.-W. Moon, *J. Mater. Chem. C*, 2015, **3**, 644.
11. P. Colomban, *Proton Conductors: Solids, Membranes and Gels–Materials and Devices, in Chemistry of Solid State Materials*, Cambridge University Press, Cambridge, UK, 1992, vol. 2.
12. (a) Y. Q. Jiao, C. Qin, X. L. Wang, F. H. Liu, P. Huang, C. G. Wang, K. Z. Shao and Z. M. Su, *Chem. Commun.*, 2014, **50**, 5961; (b) Y. Q. Jiao, C. Qin, X. L. Wang, C. G. Wang, C. Y. Sun, H. N. Wang, K. Z. Shao and Z. M. Su, *Chem.–Asian. J.*, 2014, **9**, 470; (c) C. Streb, *Dalton Trans.*, 2012, **41**, 1651.
13. J. I. Pankove, *Optical Processes in Semiconductors*, Prentice-Hall, Inc., Englewood Cliffs, NJ, 1971, pp. 34.
14. (a) X. Y. Wu, X. F. Kuang, Z. G. Zhao, S. C. Chen, Y. M. Xie, R. M. Yu and C. Z. Lu, *Inorg. Chim. Acta*, 2010, **363**, 1236; (b) J. W. Zhao, Y. Z. Li, F. Ji, J. Yuan, L. J. Chen and G. Y. Yang, *Dalton Trans.*, 2014, **43**, 5694; (c) H. Y. Zhao, J. W. Zhao, B. F. Yang, H. He and G. Y. Yang, *CrystEngComm*, 2013, **15**, 8186.